NMR in Biomedicine

WILEY

NMR IN BIOMEDICINE

RESEARCH ARTICLE

In Vivo Quantitative Detection of PEGylated Macromolecules by Magnetic Resonance Spectroscopy

Advait Hasabnis[1] | Yi-Chia Su[1] | Rohan Alvares[1] | Daniel P. Downes[2,3] | Huadong Zeng[2] | Joanna R. Long[2,3] | Robert S. Prosser[1,4]

[1]Department of Chemistry; Chemical and Physical Sciences, UTM, University of Toronto, Mississauga, Ontario, Canada | [2]National High Magnetic Field Laboratory, University of Florida, Gainesville, Florida, USA | [3]Department of Biochemistry and Molecular Biology, University of Florida, Gainesville, Florida, USA | [4]Department of Biochemistry, University of Toronto, Toronto, Ontario, Canada

Correspondence: Robert S. Prosser (scott.prosser@utoronto.ca)

Received: 11 December 2024 | **Revised:** 16 May 2026 | **Accepted:** 4 June 2026

ABSTRACT

Large poly(ethylene) glycol (PEG) chains are often conjugated to proteins or biomolecules to inhibit proteolytic degradation, mask immunogenic response, reduce clearance rates, and improve biodistribution of therapeutics, vaccines, drug delivery systems, and gene therapy formulations. The PEG macromolecular chain can also be used as a noninvasive reporter to track biologics in vivo by magnetic resonance spectroscopy (MRS). Rapid internal dynamics of PEG render the transverse ^{1}H spin relaxation time to be comparable to water (~0.5 s) and amenable to imaging through traditional pulsed field gradient techniques. While water signal grossly exceeds that of PEG it is possible to filter ^{1}H MRS signal of PEGylated conjugates through one of two ways—(1) stimulated echo acquisition mode (STEAM) MRS, which leverages huge differences in the diffusion of water versus PEGylated constructs, and (2) ^{13}C-edited ^{1}H MRS of fully ^{13}C-enriched PEGylated constructs. Here, we compare both approaches. A 15 kDa ^{13}C-enriched PEG chain was prepared alone, conjugated to bovine serum-albumin (BSA), and incorporated into a 52-nm-diameter PEG-poly(lactic acid) (PLA) nanoparticle. These three PEG constructs were then separately monitored in real time by ^{13}C-edited ^{1}H MRS, after introducing them into rat animal models intravenously. A ^{13}C-editing scheme was employed to monitor ^{1}H MRS PEG signal in the vasculature via a radiofrequency coil placed around the tail. An observed two-component decay of the PEG signal is attributed to perfusion and early equilibration (alpha phase) and slow clearance (beta phase). ^{13}C-PEG alone, ^{13}C-PEG-BSA, and ^{13}C-PEG–PLA nanoparticles exhibited half-lives of 38.6 min, 23.4 h, and 11.9 h, respectively. The relatively rapid clearance rates associated with the PEG–PLA nanoparticles is expected to arise from enzymatic degradation of the PLA chain. Using STEAM-based editing schemes, we then evaluated sensitivity and water suppression in diffusion-edited ^{1}H MRS for (^{12}C)-PEGylated BSA contrasting 2-, 20-, and 40-kDa PEG chains, in imaging phantom samples. Larger molecular weight PEG chains (i.e., 40 kDa) proved far superior to smaller PEG chain reporters due to reduced inhomogeneities and longer T_2, upon employing either a ^{13}C-HQMC filter or a STEAM-based diffusion filter.

Abbreviations: BSA, bovine serum-albumin; CAC, carotid artery catheter; FDA, U.S. Food and Drug Administration; HMQC, heteronuclear multiple quantum coherence; JVC, jugular vein catheter; mAb, monoclonal antibody; MRI, magnetic resonance imaging; MRS, magnetic resonance spectroscopy; NMR, nuclear magnetic resonance; PEG, polyethylene glycol; PET, positron emission tomography; PLA, polylactic acid; SE-DWI, spin echo diffusion weighted imaging; SNR, signal-to-noise ratio; SPECT, single-Photon Emission Computed Tomography; STEAM, stimulated echo acquisition mode; T_2, transverse spin relaxation time; WALTZ, wideband alternating-phase low-power techniques for zero-residual splitting.

1 | Introduction

Biologics, including monoclonal antibodies (mAbs), recombinant peptides and proteins, antibody-drug conjugates, and cell- and gene therapies, greatly enhance modern therapeutic applications [1]. Since 2018, over 30% of all FDA-approved drugs have been biologics, underscoring their growing importance [2]. Despite their clinical importance, characterizing their pharmacokinetics (absorption, distribution, metabolism, and excretion) remains a significant challenge, particularly since they are often unique to a specific biologic [1]. Traditional monitoring in animal models often relies on radiolabeling for SPECT or PET imaging, yet these methods face hurdles regarding radioligand accessibility, stability and lifetime of the probe, radiolabel licensing, and perturbations to the innate biodistribution of the unlabeled biologic [1, 3–5]. Furthermore, while optical methods provide high resolution, they are fundamentally limited by depth penetration in diverse biological environments. Here we consider the use of Magnetic Resonance Spectroscopic (MRS) methods to measure drug half-lives and quantify concentrations across bodily compartments, especially in the context of their application toward rapidly evolving therapeutic modalities [6].

Biologics, including peptide and protein therapeutics, vaccines, drug delivery systems, and gene therapy formulations, are often conjugated to the polymer, poly (ethylene) glycol (PEG), to inhibit proteolytic degradation, mask immunogenic response, reduce clearance rates, and improve biodistribution [7–11]. We propose that poly (ethylene) glycol (PEG), which is biocompatible and weakly immunogenic, can serve as a powerful endogenous reporter. Unlike most biologics, which generally cannot be directly detected via ^{1}H MRS due to molecular-weight-dependent line broadening, the PEG chain rescues transverse relaxation times and the possibility of MRS. Its ethylene oxide protons undergo rapid chain isomerization, resulting in ^{1}H T_2 relaxation times (~0.5–0.6 s) that remain long and largely independent of the molecular weight of the conjugate. This distinctive spectroscopic signature, confined to 3.6 ppm, allows PEG signal to be isolated from background water and fat at high magnetic fields. Here, we evaluate and compare two specific editing schemes designed to eliminate background interference and maximize sensitivity: ^{13}C-edited ^{1}H MRS utilizing fully ^{13}C-enriched PEG and diffusion-edited ^{1}H MRS leveraging the large difference in translational diffusion rates between fast-moving water and slow-moving PEGylated constructs. By applying these methods to in vivo rat models and phantom samples, we demonstrate the ability to monitor vascular clearance and organ-specific accumulation in real time, validating the results against traditional invasive blood sampling.

2 | Experimental

^{13}C-Ethylene oxide was purchased from Sigma-Aldrich (ISOTEC, Old Bridge, NJ, USA). Bovine serum albumin (BSA) was purchased from BioShop Canada Inc. (Burlington, ON, Canada). Sodium cyanoborohydride, potassium tert-butoxide, DL-lactide, stannous octoate, the anhydrous solvents acetone, toluene, tert-butanol, dimethyl sulfoxide (DMSO) and D_2O (99.9%) were purchased from Sigma-Aldrich (Oakville, ON, Canada). Phosphoric acid, NH_4OH, NaCl, NaOH, HCl, chloroform, dichloromethane, toluene, and diethyl ether were obtained from Caledon Laboratories Ltd. (Georgetown, ON, Canada). 4-Chlorobutyrladehyde diethyl acetal was bought from AK Scientific Inc. (Mountain View, CA, USA).

3 | Synthesis

3.1 | ^{13}C-Polyethylene Glycol (^{13}C-PEG)

^{13}C-PEG was synthesized by anionic ring-opening polymerization of ^{13}C-ethylene oxide, which resulted in incorporation of two ^{13}C nuclei per ethylene monomer [12]. Briefly, 9.5 mg potassium tert-butoxide and 13.79 g anhydrous DMSO were added to a reaction tube. A 3.03 g ^{13}C-ethylene oxide was dried over sodium metal and transferred to the reaction vessel, and the solution was stirred at 50°C for 96 h, after which the reaction was quenched with 0.1 M HCl. ^{13}C-PEG was precipitated by adding the reaction mixture into 550 mL cold diethyl ether. The precipitate was separated by centrifugation, and the pellet was washed three times with cold diethyl ether with a yield of 2.69 g. The molecular weight of ^{13}C-PEG was determined by ^{1}H NMR end group analysis, where the relative ratio of tert-butyl and alcohol end groups to PEG methylene groups indicated a mean size of 15.4 kDa.

3.2 | ^{13}C-PEG-Butyraldehyde (^{13}C-PEG-BA)

PEG-butyraldehyde was produced in two steps, where a protected aldehyde was first added to the PEG hydroxyl end group followed by a deprotection step to give the aldehyde. ^{13}C-PEG (2.1 g) was first azeotropically dried with toluene at 60°C. A mixture of the dried ^{13}C-PEG, potassium tert-butoxide (0.93 g), and 4-chlorobutyraldehyde diethyl acetal (1.09 g) in 15 mL anhydrous toluene and 4 mL anhydrous tert-butanol was refluxed at 105°C for 36 h. The reaction mixture was then dried under vacuum and dissolved in a minimum amount of DCM and added dropwise into cold diethyl ether (200 mL) to precipitate the ^{13}C-PEG-butyraldehyde diethyl acetal. The precipitate was further washed twice with cold diethyl ether and dried under vacuum.

The above precipitate was dissolved in Milli-Q water (40 mL), the pH adjusted to 3.0 using 5% phosphoric acid (~2 mL) and the solution was stirred for 12 h at room temperature. A 2.13 g of NaCl was added, the pH was adjusted to 6.8 using 1 M NaOH, and the product was extracted with chloroform (4 × 50 mL). The organic layer was dried under vacuum, washed with cold diethyl ether (2 × 45 mL) and dried again, yielding 1.99 g of product.

3.3 | ^{13}C-PEGylated Bovine Serum Albumin (^{13}C-PEG-BSA)

A 0.28 g ^{13}C-PEG-BA (18 μmoles) and 1 g BSA (15 μmoles) were dissolved in 20 mL phosphate buffered saline (10 mM phosphate, 137 mM NaCl, 2.7 mM KCl, pH 7.4) and stirred gently for 2 h at room temperature. A 9.4 mg sodium cyanoborohydride (150 μmoles) was then added, and stirring was continued for 12 h. A further 9.4 mg of sodium cyanoborohydride was added

to the reaction and stirred for another 24 h. Ammonia in water (0.1%, 12 μL) was added to quench any unreacted aldehyde. The ^{13}C-PEG-BSA conjugate was purified using size exclusion chromatography.

Size exclusion chromatography was employed using a HiLoad Superdex 200 PG column (GE Healthcare Life Sciences). ^{13}C-PEG-BSA (25 mg/mL BSA) was injected into the column and eluted with PBS, collecting 3 mL fractions. Protein elution was monitored at 280 nm, while the PEG concentration for each fraction was later determined by ^{1}H NMR. The desired fractions were pooled and concentrated (Amicon Ultra-15 Centrifugal Filter Units, 30,000 MWCO, Millipore Sigma) by centrifugation.

3.4 | ^{13}C-Peg–PLA

^{13}C-PEG–PLA copolymer in a 3:1 ratio of lactic acid to ethylene glycol units was synthesized by ring opening polymerization of DL-lactide using ^{13}C-PEG. Briefly, ^{13}C-PEG (0.25 g) and DL-lactide (0.75 g) were dried under vacuum for 24 h and dissolved in 10 mL dry toluene along with 8 μL of stannous octoate as a catalyst. The mixture was refluxed at 110°C for 24 h in a dry, inert environment (nitrogen or argon gas). The resulting mixture was dissolved in dichloromethane and added dropwise to cold diethyl ether (100 mL) to precipitate the copolymer. The precipitate was further washed with cold diethyl ether and dried under vacuum.

The composition and molecular weight of the ^{13}C-PEG–PLA copolymer were determined by ^{1}H NMR. The integral of PLA methanetriyl protons (CH-) at 5.22 pm and that of PEG protons (-OCH_2CH_2) at 3.56 ppm were used to determine the ratio of lactic acid to ethylene glycol units and hence the average molecular weight (M_n). The ratio of PEG to PLA was determined to be 1:2.94 and hence M_n = 60.7 kDa (PEG 15.4 kDa: PLA 45.3 kDa).

3.5 | Preparing and Characterizing PEG–PLA Nanoparticles (NP)

^{13}C-PEG–PLA nanoparticles were freshly prepared by the solvent evaporation method. Briefly, 10 mL acetone containing 1% w/v copolymer was added dropwise to 30 mL phosphate buffer while being stirred vigorously. This solution was stirred for two more hours under light vacuum to allow the acetone to evaporate and obtain nanoparticle dispersion. The nanoparticles were washed with water and concentrated (Amicon Ultra-15 Centrifugal Filter Units, 30,000 MWCO, Millipore Sigma) by centrifugation. The average diameter and polydispersity (PDI) of nanoparticles were measured by DLS (Zetasizer Nano-ZS, Malvern Instruments). The average diameter of the nanoparticles was 52 nm, with a PDI of 0.078.

4 | Methods

4.1 | In Vivo MRS Experiments

Data were acquired using an 11.1 T Magnex magnet with a horizontal 40-cm bore MRI scanner equipped with an Agilent VNMRS console and vnmrj4.1 software and a RRI BFG 240/120 gradient. A home-made dual-tuned ^{13}C (inner coil with ID = 10 mm) /^{1}H (outer coil with ID = 12 mm) volume coil was used and arranged around the tail. All animal experiments were approved by the Institutional Animal Care and Use Committee (IACUC) of University of Florida. Animal anesthesia was applied by ventilation of 4% isoflurane in O_2 gas in a chamber first, and was transferred to an MRI-compatible animal bed, placed into the isocenter of the magnet. Light anesthesia was maintained during the imaging procedure via an O_2/isoflurane mixture (1.0%–1.5%) delivered through a nose cone. Body temperature was maintained at 37°C using a SAI animal monitoring system and temperature controller (SA instruments, New York, NY) which also displayed and recorded heart rate, respiratory rate, and core temperature.

For clearance studies, nine female Sprague Dawley rats (160–200 g) from Charles River Laboratories with jugular vein catheterization were used. They were split into three groups of three rats each. Three groups of rats received a 1 mL bolus of either ^{13}C-PEG (50 mg/mL, group 1), ^{13}C-PEG-BSA (100 mg/mL, group 2), and ^{13}C-PEG–PLA (100 mg/mL, group 3). Rats received a single steady-rate injection of the above-mentioned solutions into the jugular vein. Rats injected with ^{13}C-PEG were scanned every ~3 min for 1 h (64 scans each) immediately after injection whereas those injected with ^{13}C-PEG-BSA and ^{13}C-PEG–PLA were scanned for the first 4 h after injection (~7 min, 128 scans each) and then twice a few hours after injection.

4.2 | Spin Echo Diffusion Weighted Imaging (SE-DWI)

Data were collected using a 7 T Biospec 70/30 USR (Bruker) with a BGA-12S gradient coil insert. All images were acquired with a 32 × 32 mm field of view (FOV) and 32 × 32 matrix for 1 mm spatial resolution in-plane. The slice thickness was 10 mm. Other imaging parameters included an echo time (TE) of 50 ms, a 3000 ms repetition time (TR), 8 transients, a gradient duration of 10 ms, a 15 ms gradient separation, and b-values of 0 and 8000 for the control and diffusion-weighted scans respectively, as shown in Figure 4E,F.

4.3 | Stimulated Echo Acquisition Mode (STEAM) MRS

Data were collected using a 11.1 T Magnex magnet with horizontal 40 cm bore MRI scanner equipped with a Bruker AV3 HD console and ParaVision 6.0.1 software and a RRI BFG-240/120 gradient coil. A home-made 2.5 × 2.5 cm saddle-shaped quadrature surface transmit coil was used for the studies. After the initial scout images to confirm the rat's bladder at the magnet isocenter, FLASH images were acquired to facilitate the voxel placement on the bladder. All spectra were acquired using the VAPOR WS-STEAM [13] sequence with voxel sizes adjusted to the size of the bladder (typical 2.5 × 2.5 × 2.5 for control to 5 × 3 × 5 mm^3 voxel after injection), 256 transients, a repetition time of 1 s and a 100 ms echo time and a mixing time of 10 ms.

4.4 | Blood Sampling Experiments

Female Sprague Dawley rats (160–200 g) from Charles River Laboratories were used. Catheters were implanted in the jugular vein (JVC) for test substance administration and carotid artery (CAC) for serial blood collection. A 1 mL samples of either ^{13}C-PEG (50 mg/mL), ^{13}C-PEG-BSA (100 mg/mL), or ^{13}C-PEG–PLA (100 mg/mL) were administered via the surgically placed JVC. Serial blood samples were collected from the CAC, and the sample volume replaced with saline. All blood samples were transferred into heparin tubes on wet ice and centrifuged within 5 min to obtain plasma. Samples were stored frozen (−80°C) until analysis.

4.5 | Sample Preparation for ^{13}C-Edited MRS and Stimulated Echo NMR Experiments of PEG-BSA

Samples 2-kDa PEG maleimide (2110 g/mol), 20 kDa PEG maleimide (20,750 g/mol), and 40-kDa PEG maleimide (39,739 g/mol) were dissolved in H_2O and stored at −20°C as stock solutions. None of these compounds were ^{13}C-labeled, and natural abundance ^{13}C-signal was used to evaluate ^{13}C-editing schemes. Commercial BSA was dissolved in 20 mM phosphate buffer (pH 6.0) with 200 mM NaCl to prepare a 150 μM solution of BSA. This solution was then pretreated with 0.1 M EDTA and 2 mM DTT at 4°C overnight, spin-concentrated in a 10 kDa (MW) cutoff centrifugal filter unit, and buffer exchanged to remove DTT over 24 h and finally stored at −20°C until use. The conjugation of PEG-maleimide and BSA was performed at 4°C for 2 weeks in 20 mM sodium acetate (pH 8.0), using 300 μM of BSA and 200 μM of PEG-maleimide. The products were then buffer-exchanged and spin-concentrated to 100 μL to remove unreacted PEG maleimide using a 10 kDa MW cutoff filter. Samples were stored at −20°C until analysis by NMR. NMR samples were prepared by combining 100 μL of PEGylated BSA with 450 μL of laked bovine blood along with 50 μL of D_2O and DMF with a final PEG-BSA concentration of 5 mM.

4.6 | Solution NMR Experiments

^{13}C-edited ^{1}H NMR spectra were acquired at 25°C using 768 scans via a TANGO-HMQC sequence [14] on a 600 MHz Varian Inova spectrometer. A 13 μs 90° ^{1}H excitation pulse was used along with a 2 s repetition time, and a WALTZ broadband ^{13}C-decoupling scheme [15] during an 85 ms acquisition period. Despite the HMQC filter, a low receiver gain was required to accommodate the sizeable ^{1}H water signal. A ^{1}H stimulated echo diffusion-edited ^{1}H NMR sequence was also used on the identical sample with considerably better success suppressing the water signal. In this case, a gradient refocusing time of 1.5 ms, using two 1-ms gradient encoding pulses at a strength of 33 G/cm, and an intervening longitudinal mixing period of 197 ms was used to attenuate the solvent background signal, as shown in Figure S1. In total, 256 scans and a repetition time of 2 s were used in the stimulated echo sequence.

5 | Results

Figure 1A illustrates an HMQC filter to remove water and background (^{12}C)-fat and lipid signal, commonly observed in ^{1}H MRS. Here, differencing the resulting signal, after alternating the carbon pulse phases from “x” to “-x” in alternate scans, will result in canceling out non-^{13}C-coupled signal. The delay τ is set to $1/2J_{CH}$ (J_{CH} = 144 Hz) to efficiently transfer ^{1}H magnetization to ^{13}C and back to ^{1}H for detection. Figure 1B shows the two-scan sequence where the phase of non-^{13}C-coupled protons is inverted and cancelled out. The combined delay of 2τ (= 6.94 ms) which is a small fraction of

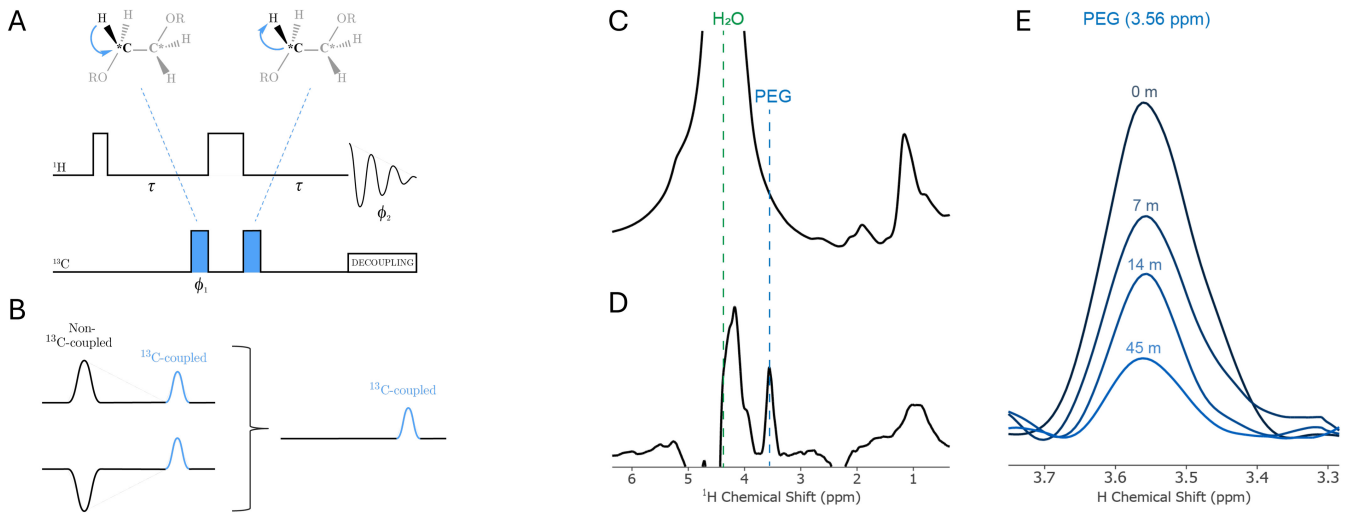

FIGURE 1 | ^{1}H-observe ^{13}C-editing MRS via an HMQC scheme. (A) In the heteronuclear multiple-quantum coherence (HMQC) scheme, ^{1}H magnetization is passed through ^{13}C during the first τ delay and returned to ^{1}H after the second ^{13}C 90° pulse. (B) By inverting the phase, ϕ_1, of the ^{13}C 90° pulse, in alternate scans, non-^{13}C-coupled ^{1}H signal will alternate in sign, allowing for background, non-^{13}C-coupled signal to be averaged away. (C) ^{1}H MRS spectra of a rat tail immediately after injection of ^{13}C-PEG. (D) ^{13}C-filtered ^{1}H MRS spectra of a rat tail immediately after ^{13}C-PEG injection, plotted on the same scale as that in (C). (E) ^{13}C-filtered ^{1}H MRS spectra of ^{13}CPEG (MW = 15.4 kDa) obtained at 0, 7, 14, and 45 min after ^{13}C-PEG injection. MRS signal was obtained via a detection coil fitted around the tail of a rat.

the T_2 relaxation time of the PEG protons (~600 ms), results in negligible signal attenuation caused by T_2 relaxation. In contrast, fat has a T_2 on the order of 80 ms, in which case a significant proportion of natural abundance fat signal will be lost either through relaxation or frequency-selective excitation and filtering pulses. Upon introducing ^{13}C-PEG intravenously to an animal at a concentration of 50 mg/mL, ^{1}H MRS signal was monitored using a coil placed around the tail. In the absence of the filter (Figure 1C), ^{1}H MRS signal is dominated by water. Upon using the ^{13}C-filter (Figure 1D), the background water resonances are significantly suppressed and the PEG resonance at the same concentration is easily visible over the range of times studied. ^{13}C-PEG of average weight (M_n) 15.4 kDa was synthesized from ring-opening polymerization of ^{13}C-ethylene oxide as described in the experimental methods [12]. This ^{13}C-PEGylated species was then used to monitor blood clearance in a rat animal model. Upon intravenous administration into three live rats at a concentration of 50 mg/mL, the ^{13}C-edited MRS signal was monitored in real time, as shown in Figure 1E. In all cases, the ^{13}C-PEG signal is clearly discriminated from water and monitored for up to 45 min.

^{13}C-PEG was separately conjugated to bovine serum albumin by reductive amination. In addition, a ^{13}C-PEG–PLA copolymer in a 1:3 ratio of lactic acid to ethylene glycol units was synthesized by ring-opening polymerization of DL-lactide using the identical ^{13}C-PEG source. ^{13}C-PEG–PLA nanoparticles were next freshly prepared by the solvent evaporation method [16]. The average diameter of the nanoparticles, determined by dynamic light scattering (DLS), was 52 nm. These three PEGylated formulations were intravenously injected into three different groups of rats and ^{13}C-edited ^{1}H MRS of the rats' tails were recorded at specific time intervals after injection. Figure 2A illustrates the use of an MRI coil focused on the tail of the animal such that the vasculature can be efficiently sampled in real time. Figure 2B shows the ^{13}C-edited ^{1}H MRS signal where PEG and water are completely separated and ^{13}C-PEG can be quantified in real-time over a large dynamic range during a 100-min observation period. Blood clearance profiles for the three compounds are shown in Figure 2C in semi-logarithmic plots. Notably, the larger ^{13}C-PEG-BSA and ^{13}C-PEG–PLA exhibit a single exponential relationship between concentration and time where concentration can be expressed as $C_t = C_{initial} \times e^{-k_{el}t}$. This "one compartment model" is the simplest pharmacokinetic model. In this scenario, an intravenous bolus of a molecule rapidly partitions to the entire vasculature and is then gradually cleared following a first-order, single exponential decay. A semi-logarithmic plot would depict a linear decline in log-concentration with a slope corresponding to the clearance rate. This is the observed pattern for ^{13}C-PEG-BSA and ^{13}C-PEG–PLA NP. Figure 2D represents a ^{1}H MRI cross section of the rat tail, where arteries and veins are indicated.

In contrast to the results for the larger PEG-BSA and PEG–PLA NP conjugates, the clearance profile for ^{13}C-PEG alone reveals a distinct biphasic relationship, as shown in Figure 2C. In this case, ^{13}C-PEG rapidly distributes within

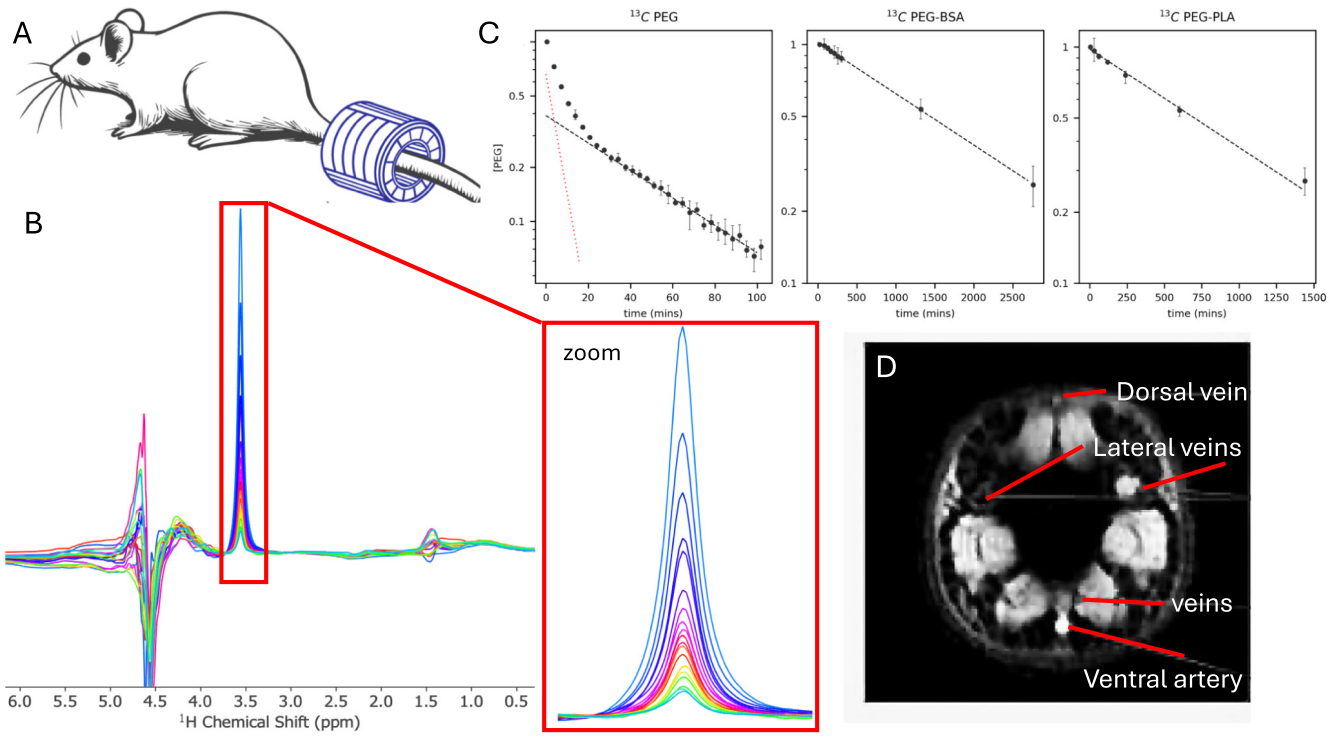

FIGURE 2 | Real-time MRS of PEGylated formulations in live animals. (A) Schematic representation of a rat with a home-made dual-tuned ^{13}C (inner coil with ID = 10 mm) /^{1}H (outer with ID = 12 mm) MRS volume detect coils arranged around the tail. (B) Real-time ^{13}C-edited ^{1}H MRS spectra collected over 100 min, after injecting 1 mL of a 50 mg/mL bolus of ^{13}C-PEG intravenously. (C) MRS signal intensity of ^{13}C-edited PEG versus time for 15.4 kDa ^{13}C-PEG alone, conjugated to BSA, or conjugated to PLA in a PEG–PLA 1:3 nanoparticle (from left to right, respectively). The clearance profile of PEG alone is fit to a two-compartment pharmacokinetic model. Error bars indicate the range of values from $N = 3$ rats. (D) ^{1}H MRI cross section of the rat tail, illustrating vascular tissue.

the bloodstream and highly perfused organs (central compartment) in an alpha phase before gradually distributing to other body tissues and less perfused organs (peripheral compartment). Consequently, the initial steeper decline in PEG concentration (indicated by the red dotted line in Figure 2C) reflects a combination of clearance (black dashed line) and equilibration with the peripheral compartment. This phase ends when a pseudo-equilibrium is established between central and peripheral compartments [17, 18]. This is followed by a beta phase of gradual decrease in concentration primarily attributed to clearance. The terminal half-life is thus indicated by the slope of the beta phase. This observed pattern aligns with the widely accepted "two compartment model" in pharmacology, as depicted in Figure 3 [17, 18]. By leveraging the signal amplification from PEG protons, we were able to capture the alpha phase due to the "real-time" nature of the MRS experiment. In this case, a short repetition time of 3 s with an $n = 64$ enabled recording of individual spectra at approximately 3-min intervals.

While ^{13}C-edited MRS provides the requisite differentiation between water and PEGylated constructs, the spectra reveal a significant water background even after filtering. Ultimately, this background signal greatly constrains overall sensitivity and limits of detection. One alternative to ^{13}C-filtering is diffusion-weighted imaging (DWI), where we rely on either a spin-echo [19, 20] or a stimulated echo [21–24] which can be used to cancel water while retaining ^{1}H signal from PEG. These PEGylated constructs typically exhibit comparable T_1 and T_2 relaxation times to water, but are distinguished by their translational diffusion rates, which are hundreds of times greater than water. Spin-echo DWI (SE-DWI) uses paired diffusion gradients and a spin-echo to differentiate water from PEG [22, 25–28]. Figure 4A shows a regular ^{1}H MRI two-dimensional (10 mm) slice for phantom samples containing PEG, BSA-PEG, or serum. The images appear constant since the vast majority of proton signal arises from bulk water. This is contrasted with STEAM spectra obtained from specific voxels within two PEGylated samples as shown in Figure 4B,C. STEAM spectra clearly enable significant suppression of background water signal while preserving slow diffusing species such as PEG or PEG-BSA. In our hands, the limit of detection appears to hover around 1 mg/mL (~16 μM) BSA-PEG in 2 scans. Stimulated Echo Acquisition Mode (STEAM) diffusion-weighted MRS can in principle achieve even greater cancellation of water than that achievable from SE-DWI, since long mixing periods (TM) can be employed without appreciable loss of signal for very slowly diffusing (and long T_1) species [24]. A range of conditions is explored on an imaging phantom, showing the resulting water and PEG signals from STEAM-based spectra in Figure S2. Figure 4D reveals ^{1}H STEAM images of the phantom samples containing 8 or 74 mg/mL PEG-BSA or 82 mg/mL 100 kDa PEG as a function of a gradient diffusion filter, $b = \gamma^2 g^2 \delta^2 (T_M - \delta/3)$. For high values of b ($> 800\ s/mm^2$), the imaging signal arises principally from PEG. Figure 4E,F depict spin-echo diffusion weighted imaging (SE-DWI) results for 10 mm slices of 1:3 PEG–PLA nanoparticles, as a function of mass concentration of nanoparticle (NP), where the diffusion filter, b, is effectively zero in the left panel (4E) and 8000 in the right panel (4F). In the absence of a spin-echo diffusion filter, the image is dominated by water. However, the diffusion filter is also quite effective at masking bulk water.

Anatomical MRI images of a rat showing the bladder region in a voxel are shown in Figure 5A. Corresponding STEAM diffusion-weighted MRS on rat bladders before and 1 h after intravenous injection of a 1 mL bolus of PEG–PLA NPs (50 mg/mL NP) is shown in Figure 5B. In this case, the water signal was additionally attenuated through a VAPOR solvent suppression scheme, which compensates for B_1 inhomogeneities in the water saturation pulses [29, 30]. STEAM spectra were acquired over a period of only 5 min. While preliminary, this result demonstrates the potential to quantify PEGylated biologics in a specific organ.

To evaluate the relative sensitivity of various PEGylated biologics, using either ^{13}C-editing or diffusion-weighted schemes we first prepared three samples consisting of PEGylated BSA in serum, where the PEG chain molecular weight was either 2, 20, or 40 kDa. While linewidths normally scale with molecular weight, rapid isomerizations associated with PEG may in principle cancel line broadening resulting from slower

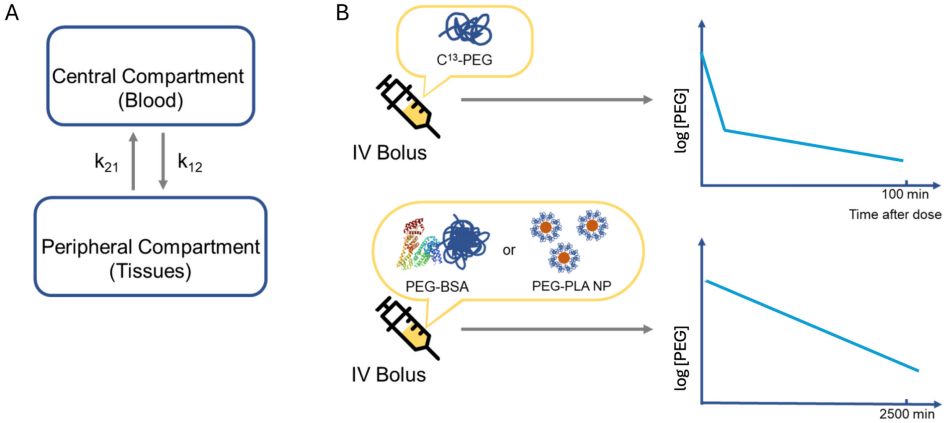

FIGURE 3 | Schematic representation of single-compartment and two-compartment pharmacokinetic models with corresponding plots of plasma concentration over time after an intravenous bolus. (A) The 1- and 2-compartment models associated with intravenous administration of PEGylated species. (B) Typical vascular clearance profiles associated with small and large PEGylated constructs (top and bottom panels respectively). A pronounced two-compartment clearance profile including the alpha phase can be seen for PEG because of the high sensitivity per unit time and the short repetition time of 3 s, enabling spectra to be recorded at 3-min intervals.

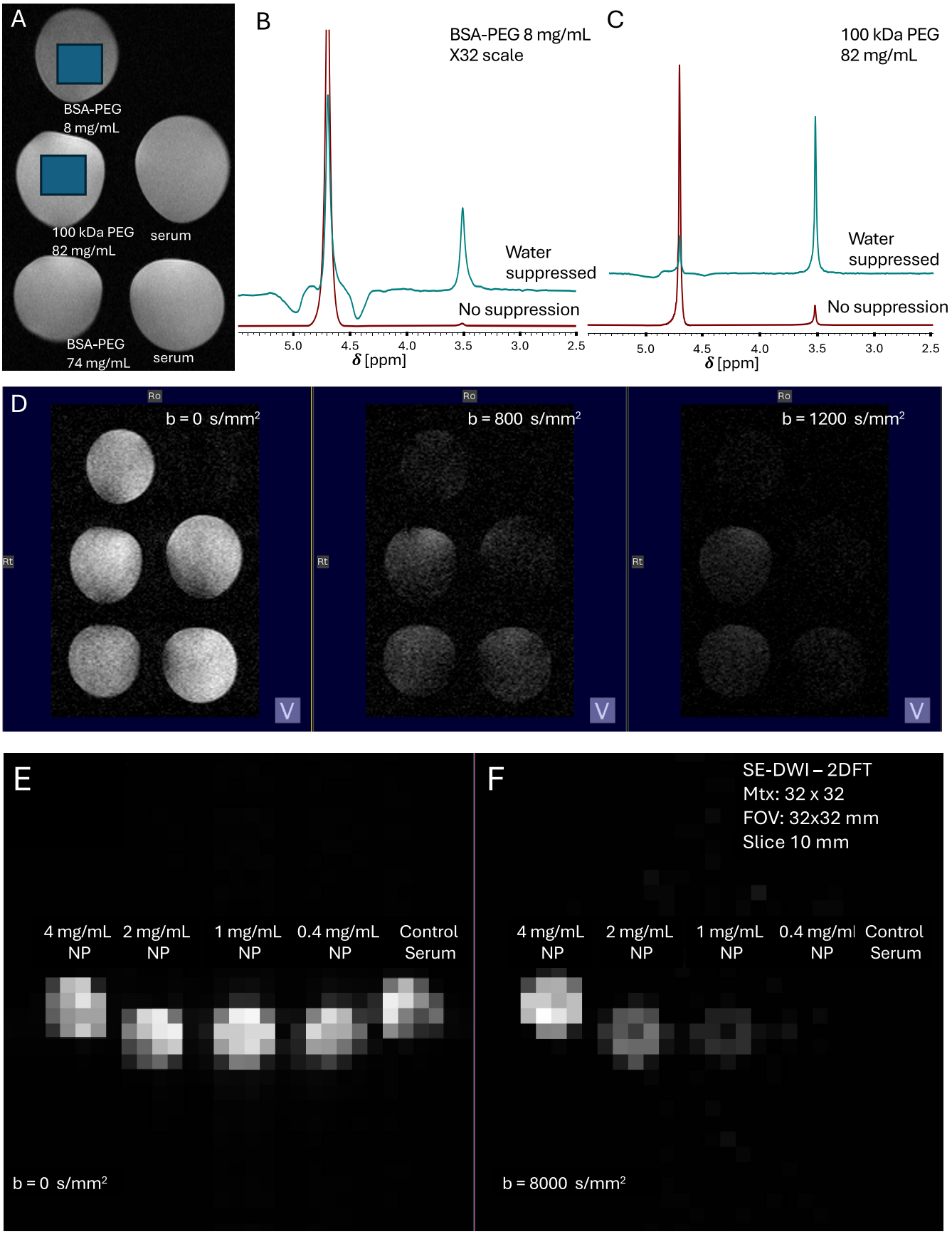

FIGURE 4 | Legend on next page.

FIGURE 4 | Spin-echo Diffusion Weighted Imaging (SE-DWI) and MR-spectroscopy of PEG and BSA-PEG in phantoms. (A) Regular ^{1}H MRI of a 1 mm slice of BSA-PEG, PEG alone, or water. In the absence of a spin-echo diffusion filter the image is dominated by water. (B) Corresponding STEAM spectra from imaging voxel shown in blue in A for 8 mg PEG-BSA. Spectra without water suppression are also shown. (C) Corresponding STEAM from imaging voxel shown in blue in A for 82 mg 100 kDa PEG. Spectra without water suppression are also shown. (D) STEAM imaging of the phantom samples shown in A as a function of the diffusion weighting parameter $b = \gamma^2 g^2 \delta^2 (T_M - \delta/3)$. Here nt = 2, echo time = 50 ms, slice thickness = 1 mm, FOV = 36 × 24 mm, matrix size = 192 × 128 and b = 0, 800, and 1200 s/mm^2 from left to right. (E) Spin-echo diffusion weighted imaging (SE-DWI) results for 10 mm slices of 1:3 PEG–PLA nanoparticles, as a function of mass concentration of nanoparticle (NP), where the diffusion filter, b, is zero. (F) As in E with b = 8000 s/mm^2.

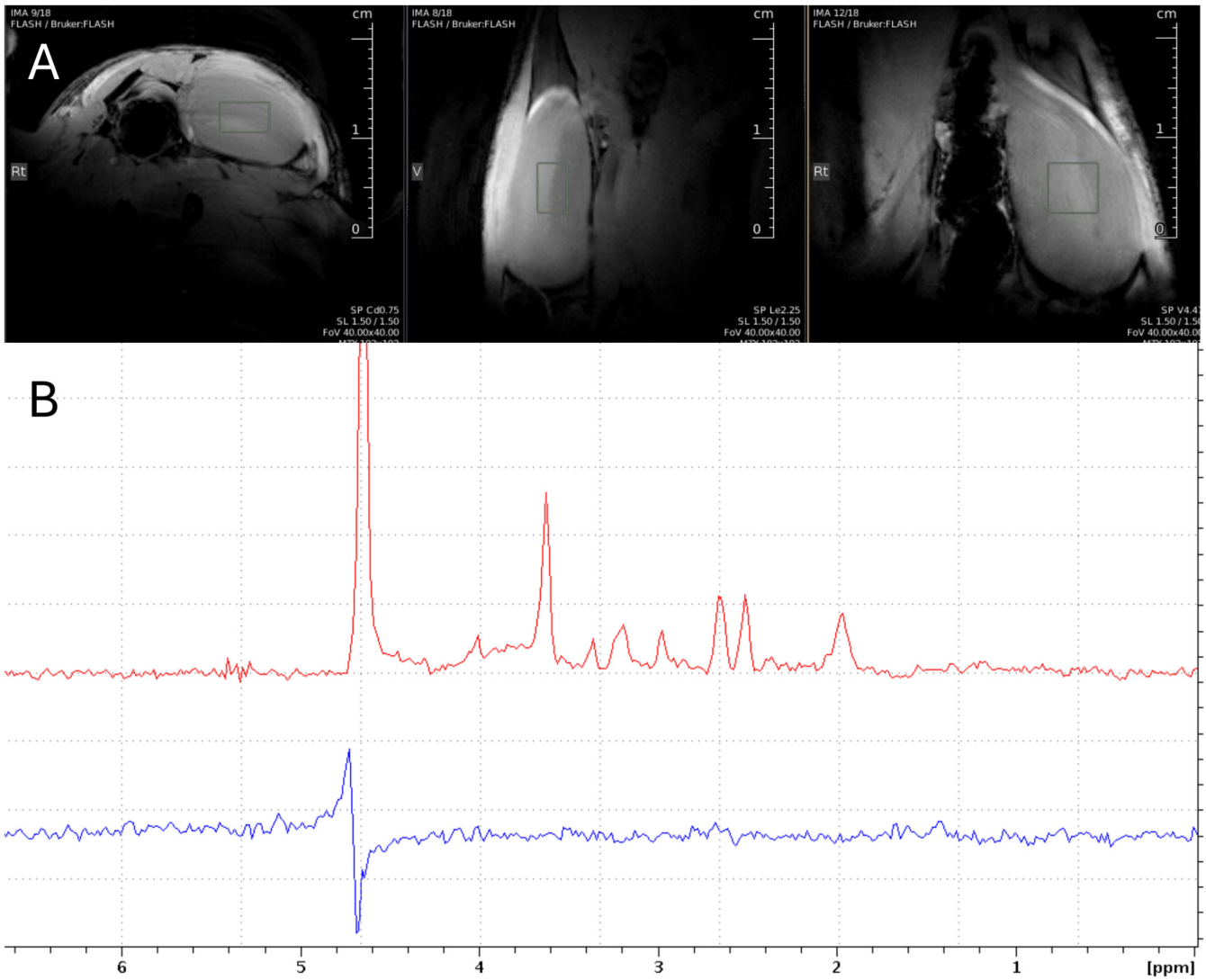

FIGURE 5 | Bladder imaging and MRS. (A) An MRI showing the anatomy of the bladder (highlighted in the voxel) and surrounding tissue. (B) STEAM MR spectrum of a rat bladder before (blue) and 3 h after (red) an intravenous injection of a PEG–PLA (1:3) nanoparticle dispersion (1 mL, 50 mg/mL concentration). Water signal was further suppressed in this experiment using a VAPOR saturation scheme and the spectrum was obtained from 258 scans across a 5 × 3 × 5 mm^3 voxel (TR = 1 s and TE = 100 ms).

overall tumbling of the aggregate. We therefore sought to evaluate water cancellation alongside PEG lineshape analysis for each of the three constructs, using either the ^{13}C-editing or ^{1}H stimulated echo. Maleimide-functionalized linear PEG chains of varying masses were separately conjugated to BSA, as described in the Materials and Methods. None of these samples were ^{13}C enriched. Equivalent mass concentrations (1 mg/mL) of dispersions of PEG-BSA derivatized with 2 kDa PEG, 20 kDa PEG, or 40 kDa PEG were characterized using ^{13}C-based editing (HMQC) and ^{1}H diffusion-editing (stimulated echo; Figure S1). Figure 6A shows the corresponding ^{13}C-edited spectra of the three PEG-BSA conjugates in serum. Each sample also contains equivalent concentrations of dimethyl formamide (DMF) as a reference. Note that the PEG linewidth surprisingly seems to improve with the molecular weight of the PEG chain or the conjugate and that the sensitivity also

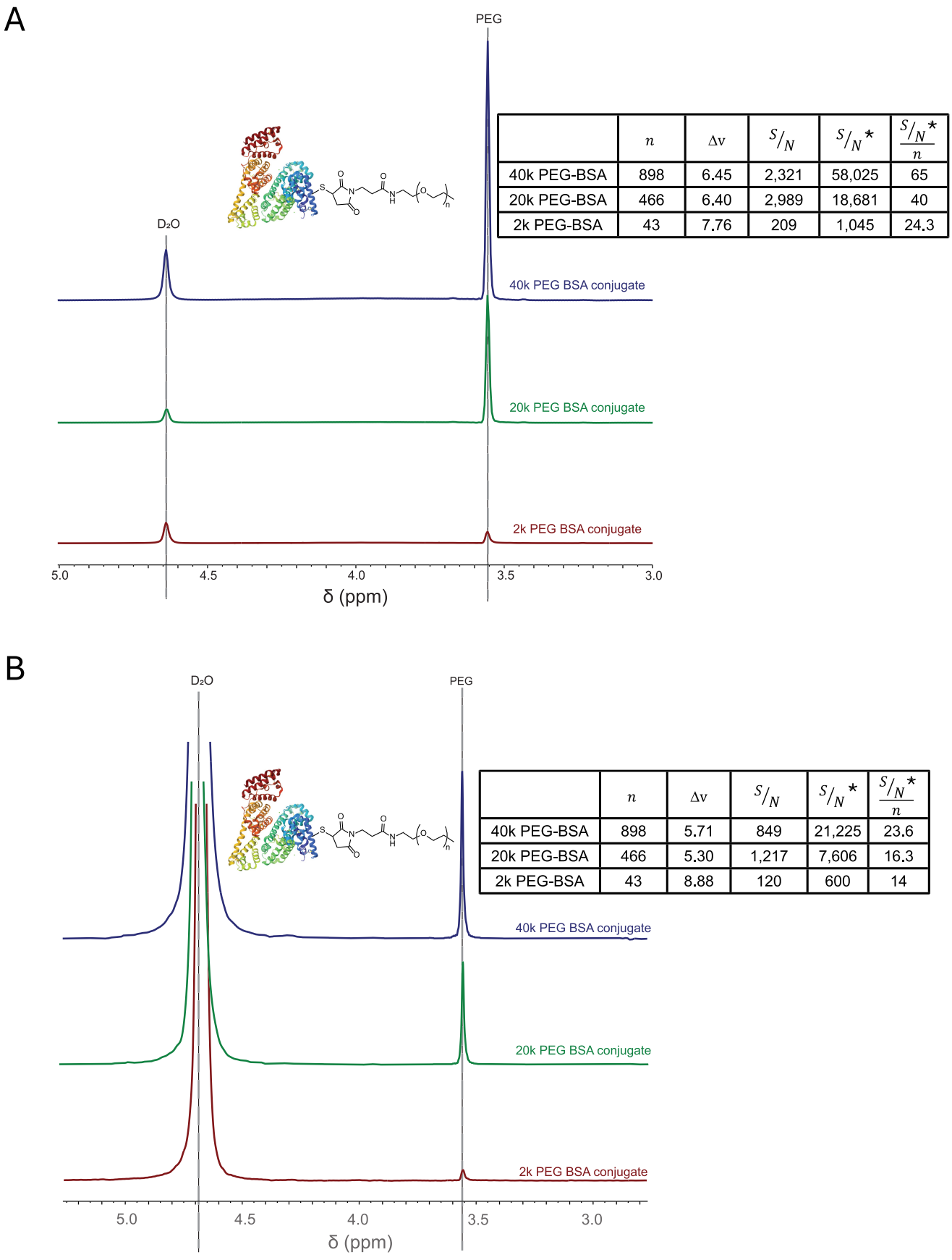

	n	Δv	S/N	S/N^*	$\frac{S/N^*}{n}$
40k PEG-BSA	898	6.45	2,321	58,025	65
20k PEG-BSA	466	6.40	2,989	18,681	40
2k PEG-BSA	43	7.76	209	1,045	24.3

	n	Δv	S/N	S/N^*	$\frac{S/N^*}{n}$
40k PEG-BSA	898	5.71	849	21,225	23.6
20k PEG-BSA	466	5.30	1,217	7,606	16.3
2k PEG-BSA	43	8.88	120	600	14

FIGURE 6 | ^{13}C HMQC-edited and stimulated echo-filtered ^{1}H NMR spectra of PEG-BSA in serum. (A) Using a ^{13}C HMQC filter and phase cycling, water can be suppressed while the PEG signal can be simultaneously observed and is noted to scale with PEG length at equal mass concentrations. (B) Using a ^{1}H stimulated echo diffusion filter, water signal is significantly suppressed while PEG signal is now clearly observed and scales with PEG length. Note that in both cases, very large PEG conjugates exhibit improved linewidths, translating into even greater enhancements in S/N.

correspondingly improves greatly with the relative concentration of methylene protons. Figure 6B shows the stimulated echo-edited spectra for the identical samples from panel A, where a spin echo delay (2 τ) of 3 ms, a gradient pulse duration of 1 ms, and a total mixing time, Δ, of 200 ms were used. Under these conditions, the water signal is nearly eliminated while the resulting PEG signal for 20 kDa PEG-BSA is essentially unaffected. In comparing water suppression between the two schemes, significant artifacts are still present when using the ^{13}C-HMQC filter, resulting in a reduced dynamic range and the need to use a lower receiver gain.

6 | Discussion

Magnetic Resonance Imaging (MRI) is routinely used in anatomical imaging, offering unparalleled capabilities in delineating soft tissues, primarily via water-based contrast mechanisms. MRS excels in quantifying metabolites, showcasing its potential beyond traditional contrast-based imaging [31–34]. Generally, site-specific quantification of metabolites by MRS relies on unique chemical shift and scalar coupling signatures and modest transverse relaxation times of the molecule of interest, since pulsed field gradients are used to spatially encode MRS signals during transverse magnetization evolution periods. However, most biologics are difficult to detect by traditional ^{1}H MRS since their linewidths which scale with molecular weight, greatly limit their detection. In contrast, poly (ethylene) glycol adopts a dynamic, disordered, and highly hydrated state in solution [35]. Consequently, the ^{1}H T_2 relaxation times of the ethylene oxide protons are on the order of 0.5–0.6 s due to significant motional averaging through chain isomerizations. As discussed below, these long relaxation times are generally independent of the molecular weight of the PEG chain, or the PEG-biologic conjugate beyond PEG molecular weights of 1 kDa. This suggests that MRS of PEGylated biologics might be possible, particularly if editing schemes can be simultaneously employed to eliminate background signals of water and fat. Conveniently, the ^{1}H PEG proton signal is confined to 3.6 ppm, where it is distinct from water and fat at sufficiently high magnetic fields (i.e., ≥ 7 T). Moreover, the molecular weights of PEGs used with biologics, vaccines, and drug delivery systems typically range from 5 kDa to 60 kDa, which facilitates high local spin concentrations and enhanced signal-to-noise ratio (SNR) for MRS detection. Two editing schemes to differentiate PEG from water and fat—namely ^{13}C-editing (in cases where the PEG is ^{13}C-enriched) or diffusion-weighted editing—are evaluated in this study.

In vivo ^{1}H magnetic resonance spectra of the body typically show a large background signal from water (~4.7 ppm) and multiple resonances from fat and tissues in the aliphatic region (0–2 ppm). These background resonances are intense compared to the signal from molecules present in low concentrations, such as metabolites, therapeutics, drug delivery systems, or vaccine formulations. In cases where the biologic of interest is PEGylated, the PEG chain may be replaced by ^{13}C-enriched PEG. This provides two key advantages. Firstly, the ^{1}H MRS PEG protons appear at a chemical shift of over 1 ppm upfield from water, which is distinct from the background water and fat signals. Additionally, the rapid isomerizations of PEG result in a narrow line width. For instance, a 20-kDa PEG chain consists of 454 monomers (1800 methylene protons) and exhibits a T_2 relaxation time of approximately 600 ms at 600 MHz [36]. Secondly, applying an HMQC filter allows for improved discrimination of PEG by reduction of the background water and fat, as shown in Figures 1 and 2, where signal from ^{13}C-PEG and ^{13}C-PEGylated BSA can be discriminated in real time [12].

6.1 | ^{13}C-PEG and Editing Schemes

The half-lives of ^{13}C-PEGylated constructs are estimated from the MRS experiments are summarized in Table 1. ^{13}C-PEG has the shortest half-life of 38.6 min as calculated from the β-phase. The corresponding excretion rate, $k_{el} = 0.018\ min^{-1}$, is roughly twice that observed previously using gamma-ray imaging of ^{125}I-radiolabeled 20 kDa PEG in mice [17]. While mice would normally be expected to exhibit higher clearance rates, due to their higher metabolic rate and renal function, it is also possible that the tryptamine functionalization used to radiolabel PEG resulted in slower clearance rates over PEG alone. Tryptamine-PEG conjugates are more likely to exhibit greater interactions with plasma proteins and tryptamine would also contribute a degree of hydrophobicity to the conjugate, thereby influencing both α- and β-phase pharmacokinetics and clearance pathways. Note that the conjugation of BSA to ^{13}C-PEG extends the half-life from 38.6 min to 23.4 h. This rate is similar to rates measured via γ-ray imaging studies in mice using ^{125}I-radiolabeled PEG-HSA with a 20 kDa PEG conjugate [37]. In this study, the authors estimated the α- and β-phase half-lives to be 0.8 h and 22.5 h, respectively. Moreover, PEGylation was observed to double the half-life of ^{125}I-radiolabeled HSA. The authors also estimated the hydrodynamic radius of PEG-HSA to be 50.7 nm while that of HSA was estimated to be 7.8 nm [37]. In the current study, we also evaluated clearance rates of ^{13}C-PEG–PLA nanoparticles, whose half-life was estimated to be 11.9 h. While these nanoparticles, whose diameters are estimated to be 52 nm, are very large compared to the renal cut-off, PEG–PLA is known to be highly susceptible to enzymatic degradation of the PLA block [38, 39]. Thus, the enhanced clearance, relative to that observed with PEG-BSA, is expected to be a consequence of continual degradation of the PLA components.

Accounting for the molecular weights of PEG (15.4 kDa), PEG-BSA (81.9 kDa), and PEG–PLA nanoparticles (60.7 kDa), and the

TABLE 1 | Half-life of three ^{13}C-PEG species as determined by the real-time, in vivo ^{13}C-filtered ^{1}H MRS technique and by serial blood sampling followed by ^{13}C filtered ^{1}H NMR. Error bars were derived from N = 3 samples.

PEG species	$t_{1/2}$ from in vivo ^{13}C-edited ^{1}H MRS	$t_{1/2}$ from serial blood sampling
^{13}C-PEG	38.6 ± 1.0 min	38.8 ± 0.6 min
^{13}C-PEG-BSA	23.4 ± 2.9 h	24.4 ± 3.1 h
^{13}C-PEG–PLA NP	11.9 ± 0.4 h	11.2 ± 0.4 h

average blood volumes for Sprawley rats (~12 mL), we can approximate the initial PEG concentrations in the blood clearance study to be 4 mg/mL ^{13}C-PEG (1 mL bolus of 50 mg/mL), 8 mg/mL ^{13}C-PEG-BSA (1 mL bolus of 100 mg/mL), and 8 mg/mL ^{13}C-PEG–PLA (1 mL bolus of 100 mg/mL) in the vasculature. Note that for PEG-BSA, this corresponds to an initial concentration of 100 μM, which fell roughly 5-fold over the time course of the experiment. This at least establishes some sense of potential limits to ^{13}C-edited MRS of PEGylated biologics or proteins of interest in the vasculature, in cases where a 15 kDa PEG tag can be employed.

The circulatory half-lives for the same three species were also measured by serial blood collection to corroborate those calculated from MR spectroscopy. The three PEG species were intravenously injected into three different groups of rats, and blood samples were collected from the carotid artery at specific time intervals. The PEG concentration was quantified ex vivo using NMR. The measured half-lives from both methods (Table 1) exhibited a close correspondence, indicating the reliability and accuracy of the noninvasive MRS approach. A slight discrepancy in the half-life (~6%) estimation was observed for the ^{13}C-PEG–PLA nanoparticles. This disparity can be attributed to the preparation of fresh nanoparticles on different days for the two experiments, with the ^{13}C-PEG having a high polydispersity leading to higher polydispersity of the nanoparticles themselves. Despite the slight variation caused by the differing preparation conditions, the overall agreement between the calculated half-lives from the noninvasive MRS technique and the invasive blood collection method underscores the robustness and validity of the noninvasive approach.

The use of ^{13}C-edited direct MRS of ^{13}C-enriched PEGylated therapeutics and delivery systems has significant potential in tracking the blood concentration of biologics and estimating circulatory half-lives with a reasonable degree of accuracy. These findings offer an effective alternative to more invasive pharmacokinetic study methods, although they come with certain limitations. This includes the requirement for ^{13}C-enriched PEG, which is more costly than unlabelled PEG, and the necessity for dual ^{1}H and ^{13}C coils, which are not universally available in clinical settings, and could limit the use of this technique.

6.2 | Spin-Echo Diffusion Weighted Imaging

Figure 4 contrasts a regular MRI image (Figure 4A) with STEAM diffusion-filtered images across a 10 mm slice and 32 × 32 field of view associated with a diffusion filtered series of PEG, BSA-PEG, and serum phantoms. Note that in Figure 4A, the series is dominated by background water while in Figure 4D, the signal appears to arise largely from the PEG component of the nanoparticle for $b \geq 800\ s/mm^2$. Figure 4B,C compare the corresponding ^{1}H spin-echo diffusion-weighted MRS of BSA-PEG (8 mg/mL) and 100 kDa PEG (82 mg/mL), both with and without water suppression. In both cases a prominent PEG methylene signal at 3.6 ppm is resolved although a residual water artifact generally survives, even with water suppression. This is also made clear in the STEAM phantom images of pegylated nanoparticles, shown in Figure 4F, using a diffusion filter of b = 8000 s/mm^2, where the water background is clearly eliminated. Our conclusion is that spin-echo DWI and MRS can both delineate water from PEG signal. Importantly, the stimulated echo is critical to attenuate water signal by effectively achieving longer evolution times, as discussed below [19, 21, 23, 24, 28].

6.3 | Diffusion-Weighted Imaging

The stimulated echo is remarkably effective at filtering water and selecting for the PEGylated constructs, largely because T_1 and T_2 of the PEG constructs (~0.5–1 s) are considerably longer than the frequency labeling period, (i.e., 2(δ+ζ) in Figure S1), while relatively little diffusional displacement takes place during the effective diffusion time, Δ, for PEG in comparison to water. In a stimulated echo pulsed field gradient, ^{1}H diffusion-edited scheme using a pair of bipolar gradient pulses, the fraction of surviving intensity (I/I_0) is given by

$$I/I_0 = exp\left[-bD\right] = exp\left[-(\gamma\delta g)^2 D(\Delta - \delta/3)\right], \quad (1)$$

where γ, δ, and g represent the gyromagnetic ratio (rad T^{-1} s^{-1}), gradient pulse duration (s), and gradient strength (T m^{-1}), respectively, while Δ (s) is the experimental diffusion mixing time and D is the diffusion coefficient (m^2 s^{-1}). Adopting parameters used to compare water filtering and signal to noise of various PEGylated constructs used in this study, ($\delta = 4\ ms$, g = 0.6 T/m, $\gamma = 42.6\ MHz/T$, and $\Delta - \delta/3 = 199.7\ ms$), we obtain $b = 1.6 \times 10^{10}$ s/m^2. Approximating the combined hydrodynamic radius (R_h) of a 40 kDa PEG chain (R_{h1} = 4–6 nm) conjugated to serum albumin (R_{h2} = 3.6 nm) as $R_h = 7 \pm 1$ nm, we can estimate, using the Stokes-Einstein equation, the diffusion constant at 20°C for PEG-BSA is 3×10^{-11} m^2/s, while water is estimated to have a diffusion constant of 2.5×10^{-9} m^2/s. In this case, the fraction of surviving water signal I/I_0 is essentially 0.0 versus $I/I_0 = 0.5$ for PEG-BSA for these experimental parameters. Clearly, this selective filtering works well because of the vastly different diffusion times of water versus PEG-BSA, while both species have comparable T_2 relaxation times. Figure 4B,C reveal the effective spectroscopic contrast that is achievable between water and PEG-BSA at concentrations as low as 8 mg/mL, using the stimulated echo (STEAM) MRS, where the voxels of origin are illustrated in the ^{1}H MRI images in Figure 4A. Figure 5 provides an in vivo equivalent, showing the result of a STEAM MRS obtained from a rat and focused on a 5 × 3 × 5 mm^3 voxel centered in the bladder, exactly 1 h after intravenous injection. Approximating the bladder volume as 1.5 mL, the maximum concentration of PEG–PLA in the bladder would be 33 mg/mL or 0.5 mM assuming everything returns to the bladder. In a 1:3 PEG–PLA nanoparticle, this corresponds to 3 mgs/mL of PEG methylene protons or 3 M PEG proton. The STEAM spectra in Figure 5 suggest that much lower concentrations of PEGylated constructs could in principle be quantified in specific tissues, depending on clearance rates and scan times.

Lastly, using a simple NMR phantom we directly compared ^{13}C-editing and diffusion-weighted filtering in a single HCN NMR probe. The resulting spectra, shown in Figure 6, were used to evaluate water cancellation and remaining ^{1}H signal originating

solely from PEGylated constructs, as a function of PEG length. This allowed us to ascertain if indeed the resulting signal-to-noise scales with the number of PEG units or if hydrodynamic radius or size in any way impedes the resulting sensitivity in either the ^{13}C-filter or the diffusion-weighted filter. The results show the HMQC filter to be inadequate as implemented in an imaging context, although in a spectroscopic sense the PEG signal is easily discriminated after water suppression through the ^{13}C-filter, as evidenced by the exquisite real-time spectra shown in Figure 2B. These experiments were also performed using the ^{13}C natural abundance fraction of PEG, suggesting that the water artifacts are effectively amplified relative to what could be achieved from a fully ^{13}C-enriched species. The pulse scheme used to select for ^{13}C-coupled signal, shown in Figure 1, results in large residual water signal in every scan, thus grossly affecting sensitivity. Here, HMQC coherence-transfer schemes could be employed to better suppress background signals and improve sensitivity, as suggested by the simple gradient-selected coherence filters shown in Figure S3 [40]. This solution should also be possible to implement in the presence of slice-selective excitation pulses or refocusing pulses in MRI or MRS schemes. Thus, in an MRS experiment such as that described in Figure 2, associated with real-time detection of ^{13}C-PEG signal in the vasculature via a tail coil, gradient coherence selection schemes could be very helpful since added water attenuation on every scan would allow for greater receiver gain and even cleaner spectroscopic separation.

From the spectral series in Figure 6A,B it is also clear that larger PEG constructs provide improved S/N. The table in the inset shows the measured absolute S/N of the ^{1}H PEG signal in the presence of either a ^{13}C-HMQC filter (on natural abundance samples) or a stimulated echo (diffusion) filter. Note in the table the two adjacent columns refer to the absolute S/N and the S/N normalized according to the actual content of PEGylated BSA ratio. In our hands, larger maleimide-functionalized PEG chains were less efficient to conjugate to BSA, as measured by Mass Spectrometry. Rather than filter the unreacted PEG components in the sample preparation phase, we simply normalized the measured S/N according to the known conjugation efficiency. This corrected S/N (S/N*) shows a significant improvement in S/N* with PEG size. Moreover, by evaluating (S/N)* per ethylene group (n), there is a surprising increasing trend in (S/N)*/n with PEG size for both the ^{13}C-edited BSA-PEG and diffusion-edited BSA-PEG. Specifically, in the case of the ^{13}C-HMQC filter, (S/N)*/n increases from 24.3 to 65 while the stimulated echo filter results in (S/N)*/n increasing from 14 to 23.6 as the PEG conjugate is increased from 2 to 40 kDa. In both cases there is also a decrease in linewidth ($\Delta\nu$) with increasing PEG size. Taken together, the PEG-BSA conjugates likely exhibit a range of natural linewidths and both the ^{13}C-filter and the diffusion filter select for the long transverse relaxation time (T_2) species. In so doing, the overall signal to noise ratio is greatly improved with longer PEG lengths. While an imaging system may not reach the same field homogeneities as an NMR system, the signal-to-noise ratio in any MRS experiment will nevertheless be very sensitive to the T_2 of the system. Therefore, in quantifying PEGylated biologics through MRS, the lesson from this experiment is that larger PEG chains will disproportionately enhance overall signal-to-noise ratios.

6.4 | Importance of PEG in Biologics, Vaccines, and Drug Delivery

Despite challenges associated with immunogenicity, cell penetration, and targeting [41, 42], PEGylation has revolutionized the field of drug delivery and the utility of biologics [7–11]. PEGylation has been successfully applied to a variety of drug classes, including proteins, peptides, and small molecules, leading to many FDA-approved PEGylated therapeutics, commonly ranging from 1 to 40 kDa, and many more in active clinical trials [43]. Indeed, the development of PEGylated liposomes used in COVID-19 vaccines heralded a new era in the use of mRNA vaccines [44]. By attaching poly(ethylene glycol) chains to therapeutic molecules or drug delivery systems, their stability, solubility, and circulation time in the body are significantly enhanced. This modification reduces immunogenicity and proteolytic degradation, thereby increasing the lifetime of the drug or biologic. In the current study, we chose model systems (PEG-BSA and PEG–PLA) that were representative of PEGylated therapeutics currently used in biomedical and therapeutic applications. While our model PEG–PLA nanoparticle was found to exhibit a hydrodynamic radius of 52 nm, many PEG–PLA nanoparticles for hydrophobic drugs have similar compositions and similar or larger sizes [45].

Alternative MRS imaging modalities, such as ^{19}F MRS, have demonstrated significant potential for imaging by leveraging the absence of endogenous ^{19}F signal in the body and the modestly long transverse relaxation times expected for fluorinated polymers [46]. Typically, perfluorinated polymer (e.g., perfluorooctyl bromide) nanoparticles or emulsions achieve detection limits on the order of mg/ml in ^{19}F MRI, although toxicity and excretion pathways at these high concentrations become a concern [47]. In contrast, extensive branched PLA–PEG nanoparticles could produce improved signal-to-noise in ^{1}H STEAM (and/or ^{13}C-editing) imaging applications since the methylene protons are equivalent and exhibit superior T_2 properties, particularly for large PEG chains. At the same time, PLA–PEG is biodegradable [9, 48]. Perfluorocarbon compounds (PFCs) guarantee a high local concentration of fluorine and have been used in cell imaging and oncology applications but are not suitable for molecular tagging since they can significantly alter the physicochemical properties of the molecule they are attached to. Thus, in the context of PEGylated biologics, it is not feasible to resort to ^{19}F MRS.

While MRS offers the possibility of real-time and site-specific quantification of PEGylated therapeutics, vaccines, and drug delivery systems, this comes at the expense of sensitivity relative to optical- and radionuclide-based imaging modalities. Positron Emission Tomography (PET) provides high sensitivity, although observation windows may be limited to 6 h, and its utility is hampered by the need for expensive, short-lived radionuclides, complicating experimental timing, and logistics [49–51]. Single Photon Emission Computed Tomography (SPECT) is more accessible but offers lower spatial resolution and sensitivity, alongside inherent limitations due to ionizing radiation exposure [3, 49, 52]. Optical methods, while providing high-resolution images with a high limit of detection, are fundamentally constrained by their limited depth penetration, rendering them less effective for monitoring biodistribution [53, 54]. Finally, all of these methods require a carrier be conjugated to the PEG chain

to incorporate the radionuclide or fluorophore, in which case biodistribution may be affected. These challenges underscore the necessity for alternative, noninvasive "probe-free" techniques capable of accurate, in-depth analysis within diverse biological environments.

7 | Conclusions and Future Directions

In this paper, we have considered the potential for PEG as a reporter in MRS experiments aimed at understanding the partitioning and clearance of PEGylated drugs, biologics, and PEGylated delivery systems. Two approaches were compared—namely the use of HMQC-based editing schemes to attenuate water and focus on the ^{13}C-coupled ^{1}H signal via MRS, or the use of diffusion-filtered ^{1}H MRS (DWI spin echo or STEAM sequences based on the stimulated echo). The former approach requires the synthesis of ^{13}C-enriched PEG conjugates and imaging probes with dual ^{1}H and ^{13}C coils. However, this made it possible to detect PEGylated constructs in the vasculature, essentially in real time, via a detection coil located around the tail of the rat. While the pulse scheme used to select for ^{13}C-coupled signal is straightforward to apply, a large residual water signal is still observed in every scan, as is the metabolite background signal. Here, gradient-based coherence-transfer schemes would better suppress background signals and improve sensitivity by allowing for significant improvements in gain [40].

In a second case, DWI MRS of a rat provided tissue-specific quantification of a PEGylated NP as it accumulated in the bladder. Using a stimulated echo filter, PEG signal could also be sensitively detected. The stimulated echo has the advantage that background metabolite and fat signal are suppressed, given the lower T_2 of fat signal and the higher diffusivity of metabolites. Of course, selective (^{1}H PEG) pulses at 3.5 ppm will further improve discrimination of PEG signal over background to the extent where even more modest magnetic field strengths (e.g., 3 Tesla) may be sufficient. Studies of ^{1}H PEG signal as a function of PEG size showed that ^{1}H linewidths were substantially reduced for higher molecular weight PEG chains (i.e., 20–40 kDa PEG). At equivalent mass concentrations of PEGylated constructs, this means that the overall signal-to-noise ratio should improve precipitously with PEG molecular weight.

Diffusion-edited imaging, and particularly MRS schemes that utilize the stimulated echo, have the potential to significantly attenuate water signal. In real-time blood or tissue sampling, such as that shown in Figure 2, there is also an opportunity to combine diffusion filters with ^{13}C-editing filters. Future applications might achieve even better filtering using shaped excitation pulses that avoid water and/or fat along with the possible combination of ^{13}C-enrichment and additional selection of PEG signal through ^{13}C HMQC coherence pathways.

Author Contributions

A.H., Y-C.S., R.A, D.P.D., and H.Z. conducted experiments. A.H., H.Z., J.R.L., and R.S.P. wrote and revised the manuscript. R.S.P. and J.R.L. supervised the project.

Acknowledgments

A portion of this work was performed in the McKnight Brain Institute at the National High Magnetic Field Laboratory's Advanced Magnetic Resonance Imaging and Spectroscopy (AMRIS) Facility, which is supported by the National Science Foundation Cooperative Agreement DMR-1644779 and the State of Florida. This research was accomplished through the generous support of the Natural Sciences and Engineering Research Council of Canada (2019-04367) in performing this research.

Funding

This work was supported by the Natural Sciences and Engineering Research Council of Canada (2019-04367) and the National Science Foundation (DMR-1644779).

Conflicts of Interest

The authors declare no conflicts of interest.

Data Availability Statement

All raw data will be provided to readers upon request, via a link at the time of publishing.

References

1. S. Shi, "Biologics: An Update and Challenge of Their Pharmacokinetics," *Current Drug Metabolism* 15, no. 3 (2014): 271–290.

2. A. C. Martins, F. Albericio, and B. G. de la Torre, "FDA Approvals of Biologics in 2022," *Biomedicine* 11, no. 5 (2023): 1434, https://doi.org/10.3390/biomedicines11051434 PubMed PMID: 37239105; PubMed Central PMCID: PMC10216111.

3. E. B. Corcoran and R. N. Hanson, "Imaging EGFR and HER2 by PET and SPECT: A Review," *Medicinal Research Reviews* 34, no. 3 (2014): 596–643, https://doi.org/10.1002/med.21299 PubMed PMID: 24037872.

4. D. Sun, W. Gao, H. Hu, and S. Zhou, "Why 90% of Clinical Drug Development Fails and How to Improve It?," *Acta Pharmaceutica Sinica B* 12, no. 7 (2022): 3049–3062, https://doi.org/10.1016/j.apsb.2022.02.002 PubMed PMID: 35865092; PubMed Central PMCID: PMC9293739.

5. K. Ball, G. Bruin, E. Escandon, et al., "Characterizing the Pharmacokinetics and Biodistribution of Therapeutic Proteins: An Industry White Paper," *Drug Metabolism and Disposition* 50, no. 6 (2022): 858–866, https://doi.org/10.1124/dmd.121.000463 DMD-MR-2021-000463. PubMed PMID: 35149542.

6. A. C. Anselmo, Y. Gokarn, and S. Mitragotri, "Non-Invasive Delivery Strategies for Biologics," *Nature Reviews. Drug Discovery* 18, no. 1 (2019): 19–40, https://doi.org/10.1038/nrd.2018.183 PubMed PMID: 30498202.

7. Y. Ikeda and Y. Nagasaki, "PEGylation Technology in Nanomedicine," in *Polymers In Nanomedicine*, eds. S. Kunugi and T. Yamaoka (Advances in Polymer Science, 2011), 115–140, https://doi.org/10.1007/12_2011.

8. P. Milla, F. Dosio, and L. Cattel, "PEGylation of Proteins and Liposomes: A Powerful and Flexible Strategy to Improve the Drug Delivery," *Current Drug Metabolism* 13, no. 1 (2012): 105–119, https://doi.org/10.2174/138920012798356934 PubMed PMID: 21892917.

9. J. S. Suk, Q. Xu, N. Kim, J. Hanes, and L. M. Ensign, "PEGylation as a Strategy for Improving Nanoparticle-Based Drug and Gene Delivery," *Advanced Drug Delivery Reviews* 99, no. Pt A (2016): 28–51, https://doi.org/10.1016/j.addr.2015.09.012 PubMed PMID: 26456916; PubMed Central PMCID: PMC4798869.

10. R. Shen and H. Yuan, "Achievements and Bottlenecks of PEGylation in Nano-Delivery Systems," *Current Medicinal Chemistry* 30, no. 12 (2023): 1386–1405, https://doi.org/10.2174/0929867329666220929152644.

11. A. Khajeei, S. Masoomzadeh, T. Gholikhani, and Y. Javadzadeh, "The Effect of PEGylation on Drugs' Pharmacokinetic Parameters; From Absorption to Excretion," *Current Drug Delivery* 21, no. 7 (2024): 978–992, https://doi.org/10.2174/1567201820666230621124953.

12. R. D. A. Alvares, J. Y. C. Lau, P. M. Macdonald, C. H. Cunningham, and R. S. Prosser, "Direct Quantitative (13) C-Filtered (1) H Magnetic Resonance Imaging of PEGylated Biomacromolecules In Vivo," *Magnetic Resonance in Medicine: Official Journal of the Society of Magnetic Resonance in Medicine/Society of Magnetic Resonance in Medicine* Apr 15 77 (2016): 1553–1561, https://doi.org/10.1002/mrm.26237.

13. D. Simicic, V. Rackayova, L. Xin, et al., "In Vivo Macromolecule Signals in Rat Brain 1H-MR Spectra at 9.4T: Parametrization, Spline Baseline Estimation, and T2 Relaxation Times," *Magnetic Resonance in Medicine* 86, no. 5 (2021): 2384–2401, https://doi.org/10.1002/mrm.28910 PubMed PMID: 34268821; PubMed Central PMCID: PMC8596437.

14. S. Wimperis and R. Freeman, "An Excitation Sequence Which Discriminates Between Direct and Long-Range CH Coupling," *Journal of Magnetic Resonance* 1984 58, no. 2 (1969): 348–353, https://doi.org/10.1016/0022-2364(84)90227-0.

15. A. J. Shaka, J. Keeler, T. Frenkiel, and R. Freeman, "An Improved Sequence for Broadband Decoupling: WALTZ-16," *Journal of Magnetic Resonance* 1983 52, no. 2 (1969): 335–338, https://doi.org/10.1016/0022-2364(83)90207-x.

16. G. Ruan and S. S. Feng, "Preparation and Characterization of Poly (Lactic Acid)–Poly(Ethylene Glycol)–Poly(Lactic Acid) (PLA–PEG–PLA) Microspheres for Controlled Release of Paclitaxel," *Biomaterials* 24, no. 27 (2003): 5037–5044, https://doi.org/10.1016/s0142-9612(03)00419-8 PubMed PMID: 14559017.

17. T. Yamaoka, Y. Tabata, and Y. Ikada, "Distribution and Tissue Uptake of Poly (Ethylene Glycol) With Different Molecular Weights After Intravenous Administration to Mice," *Journal of Pharmaceutical Sciences* 83, no. 4 (1994): 601–606, https://doi.org/10.1002/jps.2600830432 PubMed PMID: 8046623.

18. R. N. Upton, "The Two-Compartment Recirculatory Pharmacokinetic Model'an Introduction to Recirculatory Pharmacokinetic Concepts," *British Journal of Anaesthesia* 92, no. 4 (2004): 475–484, https://doi.org/10.1093/bja/aeh089 PubMed PMID: 14766714.

19. E. O. Stejskal and J. E. Tanner, "Spin Diffusion Measurements: Spin Echoes in the Presence of a Time-Dependent Field Gradient [Internet]," *Journal of Chemical Physics* 42, no. 1 (1965): 288–292, https://doi.org/10.1063/1.1695690.

20. M. Palombo, B. Bodini, F. Grussu, et al., "ESR Essentials: Diffusion-Weighted MRI—Practice Recommendations by the European Society for Magnetic Resonance in Medicine and Biology," *European Radiology* 36 (2025): 1–11, https://doi.org/10.1007/s00330-025-12033-x PubMed PMID: 41037070.

21. J. E. Tanner, "Use of the Stimulated Echo in NMR Diffusion Studies," *Journal of Chemical Physics* 52 (1970): 2523–2526, https://doi.org/10.1063/1.1673336.

22. O. M. Gonen, B. A. Moffat, P. Kwan, T. J. O'Brien, P. M. Desmond, and E. Lui, "Reproducibility of Glutamate, Glutathione, and GABA Measurements *In Vivo* by Single-Voxel STEAM Magnetic Resonance Spectroscopy at 7-Tesla in Healthy Individuals," *Frontiers in Neuroscience* 14 (2020): 566643, https://doi.org/10.3389/fnins.2020.566643 PubMed PMID: 33041761; PubMed Central PMCID: PMC7522573.

23. D. Voit, O. Kalentev, and J. Frahm, "Diffusion-Weighted Magnetic Resonance Imaging (MRI) Without Susceptibility Artifacts: Single-Shot Stimulated Echo Acquisition Mode (STEAM) MRI With Iterative Reconstruction and Spatial Regularization," *Quantitative Imaging in Medicine and Surgery* 11, no. 2 (2020): 83137–83837, https://doi.org/10.21037/qims-20-871 PubMed PMID: 33532281; PubMed Central PMCID: PMC7779911.

24. D. Gräfe, A. Päts, A. Merkenschlager, et al., "STEAM-DWI as a Robust Alternative to EPI-DWI: Evaluation in Pediatric Brain MRI," *PLoS ONE* 17, no. 5 (2022): e0268523, https://doi.org/10.1371/journal.pone.0268523 PubMed PMID: 35584126; PubMed Central PMCID: PMC9116624.

25. K. D. Merboldt, W. Hanicke, and J. Frahm, "Self-Diffusion NMR Imaging Using Stimulated Echoes," *Journal of Magnetic Resonance* 64, no. 3 (1985): 479–486, https://doi.org/10.1016/0022-2364(85)90111-8.

26. A. Marsman, V. O. Boer, P. R. Luijten, H. E. H. Pol, D. W. J. Klomp, and R. C. W. Mandl, "Detection of Glutamate Alterations in the Human Brain Using 1H-MRS: Comparison of STEAM and sLASER at 7 T," *Frontiers in Psychiatry* 8 (2017): 60, https://doi.org/10.3389/fpsyt.2017.00060 PubMed PMID: 28484398; PubMed Central PMCID: PMC5399075.

27. S. J. Holdsworth, R. O'Halloran, and K. Setsompop, "The Quest for High Spatial Resolution Diffusion-Weighted Imaging of the Human Brain In Vivo," *NMR in Biomedicine* 32, no. 4 (2019): e4056, https://doi.org/10.1002/nbm.4056 PubMed PMID: 30730591.

28. S. Ruschke and D. C. Karampinos, "Single-Voxel Short-TR Multi-TI Multi-TE STEAM MRS for Water–Fat Relaxometry," *Magnetic Resonance in Medicine* 87, no. 6 (2022): 2587–2599, https://doi.org/10.1002/mrm.29157 PubMed PMID: 35014731.

29. I. Tkác, Z. Starcuk, I. Choi, and R. Gruetter, "In Vivo ^{1}H NMR Spectroscopy of Rat Brain at 1 ms Echo Time," *Magnetic Resonance in Medicine* 41, no. 4 (1999): 649–656. Located at: WOS:000081422200002, https://doi.org/10.1002/(sici)1522-2594(199904)41:4<649::aid-mrm2>3.0.co;2-g.

30. A. Xavier, C. A. de Castro, M. E. Andia, et al., "Metabolite Cycled Liver ^{1}H MRS on a 7 T Parallel Transmit System," *NMR in Biomedicine* 33, no. 8 (2020): e4343, https://doi.org/10.1002/nbm.4343 PubMed PMID: 32515151; PubMed Central PMCID: PMC7379278.

31. M. Bittšanský, D. Výbohová, and D. Dobrota, "Proton Magnetic Resonance Spectroscopy and Its Diagnostically Important Metabolites in the Brain," *General Physiology and Biophysics* 31, no. 01 (2012): 101–112, https://doi.org/10.4149/gpb_2012_007 PubMed PMID: 22447836.

32. Z. Dong, "Proton MRS and MRSI of the Brain Without Water Suppression," *Progress in Nuclear Magnetic Resonance Spectroscopy* Apr 1 86–87, no. C (2015): 65–79, https://doi.org/10.1016/j.pnmrs.2014.12.001.

33. R. A. De Graaf, *In Vivo NMR Spectroscopy: Principles and Techniques [Internet]* (John Wiley & Sons Ltd. 560 p. Available From, 2018), https://doi.org/10.1002/9781119382461.

34. R. Kreis, V. Boer, I. Y. Choi, et al., "Terminology and Concepts for the Characterization of In Vivo MR Spectroscopy Methods and MR Spectra: Background and Experts' Consensus Recommendations," *NMR in Biomedicine* 34 (2020): e4347, https://doi.org/10.1002/nbm.4347 PubMed PMID: 32808407.

35. T. Shikata, R. Takahashi, and A. Sakamoto, "Hydration of Poly (Ethylene Oxide)s in Aqueous Solution as Studied by Dielectric Relaxation Measurements," *Journal of Physical Chemistry. B* 110, no. 18 (2006): 8941–8945, https://doi.org/10.1021/jp060356i PubMed PMID: 16671699.

36. R. D. A. Alvares, A. Hasabnis, R. S. Prosser, and P. M. Macdonald, "Quantitative Detection of PEGylated Biomacromolecules in Biological Fluids by NMR," *Analytical Chemistry* Apr 5 88, no. 7 (2016): 3730–3738, https://doi.org/10.1021/acs.analchem.5b04565.

37. T. Zhao, Y. Yang, A. Zong, et al., "N-Terminal PEGylation of Human Serum Albumin and Investigation of Its Pharmacokinetics and Pulmonary Microvascular Retention," *Bioscience Trends* 6, no. 2 (2012): 81–88, https://doi.org/10.5582/bst.2012.v6.2.81 PubMed PMID: 22621990.

38. F. Ahmed and D. E. Discher, "Self-Porating Polymersomes of PEG–PLA and PEG–PCL: Hydrolysis-Triggered Controlled Release Vesicles," *Journal of Controlled Release* 96, no. 1 (2004): 37–53, https://doi.org/10.1016/j.jconrel.2003.12.021 PubMed PMID: 15063028.

39. F. Ng, V. Nicoulin, C. Peloso, S. Curia, J. Richard, and A. Lopez-Noriega, "In Vitro and In Vivo Hydrolytic Degradation Behaviors of a Drug-Delivery System Based on the Blend of PEG and PLA Copolymers," *ACS Applied Materials & Interfaces* 15, no. 48 (2023): 55495–55509, https://doi.org/10.1021/acsami.2c13141 PubMed PMID: 38011651; PubMed Central PMCID: PMC10711724.

40. X. M. Kong, K. H. Sze, and G. Zhu, "Gradient and Sensitivity Enhanced Multiple-Quantum Coherence in Heteronuclear Multidimensional NMR Experiments," *Journal of Biomolecular NMR* 14, no. 2 (1999): 133–140, https://doi.org/10.1023/a:1004583910874 PubMed PMID: 21080254.

41. Y. Fang, J. Xue, S. Gao, et al., "Cleavable PEGylation: A Strategy for Overcoming the "PEG Dilemma" in Efficient Drug Delivery," *Drug Delivery* 24, no. 2 (2017): 22–32, https://doi.org/10.1080/10717544.2017.1388451 PubMed PMID: 29069920; PubMed Central PMCID: PMC8812578.

42. Z. Hussain, S. Khan, M. Imran, M. Sohail, S. W. A. Shah, and M. de Matas, "PEGylation: A Promising Strategy to Overcome Challenges to Cancer-Targeted Nanomedicines: A Review of Challenges to Clinical Transition and Promising Resolution," *Drug Delivery and Translational Research* 9, no. 3 (2019): 721–734, https://doi.org/10.1007/s13346-019-00631-4 PubMed PMID: 30895453.

43. Y. Gao, M. Joshi, Z. Zhao, and S. Mitragotri, "PEGylated Therapeutics in the Clinic," *Bioengineering & Translational Medicine* 9, no. 1 (2024): e10600, https://doi.org/10.1002/btm2.10600 PubMed PMID: 38193121; PubMed Central PMCID: PMC10771556.

44. E. Padín-González, P. Lancaster, M. Bottini, et al., "Understanding the Role and Impact of Poly(Ethylene Glycol) (PEG) on Nanoparticle Formulation: Implications for COVID-19 Vaccines," *Frontiers in Bioengineering and Biotechnology* 10 (2022): 882363, https://doi.org/10.3389/fbioe.2022.882363 PubMed PMID: 35747492; PubMed Central PMCID: PMC9209764.

45. E. Calzoni, A. Cesaretti, A. Polchi, A. D. Michele, B. Tancini, and C. Emiliani, "Biocompatible Polymer Nanoparticles for Drug Delivery Applications in Cancer and Neurodegenerative Disorder Therapies," *Journal of Functional Biomaterials* 10, no. 1 (2019): 4, https://doi.org/10.3390/jfb10010004 PubMed PMID: 30626094; PubMed Central PMCID: PMC6463038.

46. A. Mali, E. L. Kaijzel, H. J. Lamb, and L. J. Cruz, "19F-Nanoparticles: Platform for *In Vivo* Delivery of Fluorinated Biomaterials for 19F-MRI," *Journal of Controlled Release* 338 (2021): 870–889, https://doi.org/10.1016/j.jconrel.2021.09.001 PubMed PMID: 34492234.

47. L. Wu, F. Liu, S. Liu, X. Xu, Z. Liu, and X. Sun, "Perfluorocarbons-Based 19F Magnetic Resonance Imaging in Biomedicine," *International Journal of Nanomedicine* 15 (2020): 7377–7395, https://doi.org/10.2147/ijn.s255084 PubMed PMID: 33061385; PubMed Central PMCID: PMC7537992.

48. H. Chen and S. He, "PLA–PEG Coated Multifunctional Imaging Probe for Targeted Drug Delivery," *Molecular Pharmaceutics* 12, no. 6 (2015): 1885–1892, https://doi.org/10.1021/mp500512z.

49. F. M. Lu and Z. Yuan, "PET/SPECT Molecular Imaging in Clinical Neuroscience: Recent Advances in the Investigation of CNS Diseases," *Quantitative Imaging in Medicine and Surgery* 5, no. 3 (2015): 43347–43447, https://doi.org/10.3978/j.issn.2223-4292.2015.03.16 PubMed PMID: 26029646; PubMed Central PMCID: PMC4426104.

50. B. V. Marquez and S. E. Lapi, "Pretargeted Immuno-PET: Overcoming Limitations of Space and Time," *Journal of Nuclear Medicine* 57, no. 3 (2016): 332–333, https://doi.org/10.2967/jnumed.115.168096 PubMed PMID: 26659352.

51. M. Brandt, J. Cardinale, M. L. Aulsebrook, G. Gasser, and T. L. Mindt, "An Overview of PET Radiochemistry, Part 2: Radiometals," *Journal of Nuclear Medicine* 59, no. 10 (2018): 1500–1506, https://doi.org/10.2967/jnumed.117.190801 PubMed PMID: 29748237.

52. H. J. Lee, E. B. Ehlerding, and W. Cai, "Antibody-Based Tracers for PET/SPECT Imaging of Chronic Inflammatory Diseases," *Chembiochem* 20, no. 4 (2019): 422–436, https://doi.org/10.1002/cbic.201800429 PubMed PMID: 30240550; PubMed Central PMCID: PMC6377337.

53. A. J. Sinusas, "Multimodality Cardiovascular Molecular Imaging: An Overview," *Journal of Nuclear Medicine* 51, no. Supplement 1 (2010): 1S–2S, https://doi.org/10.2967/jnumed.109.068122 PubMed PMID: 20395344.

54. R. Matsuya, M. Kuroda, Y. Matsumoto, et al., "A New Phantom Using Polyethylene Glycol as an Apparent Diffusion Coefficient Standard for MR Imaging," *International Journal of Oncology* 35, no. 4 (2009): 893–900, https://doi.org/10.3892/ijo_00000404 PubMed PMID: 19724927.

Supporting Information

Additional supporting information can be found online in the Supporting Information section. **Figure S1:** nbm70345-sup-0001-Figures S1-S3.docx. A stimulated echo sequence used to differentiate large, PEGylated constructs from water. **Figure S2:** STEAM spectra obtained from the identical phantoms used in Figure 4, associated with PEG-BSA, showing the effects of various water suppression schemes. **Figure S3:** A gradient encoded 13C-filtered spectroscopy experiment.